Valeric acid-5-HT-dependent macrophage activation drives intestinal stem cell self-renewal

Zusen Fan (fanz@moon.ibp.ac.cn)
Chinese Academy of Sciences https://orcid.org/0000-0002-7866-8217
Pingping Zhu
Institute of Biophysics, Chinese Academy of Sciences
Tiankun Lu
Institute of Biophysics, Chinese Academy of Sciences
Jiayi Wu
Chinese Academy of Sciences
Xiaoxiao Zhu
Institute of Biophysics, Chinese Academy of Sciences
Benyu Liu
Institute of Biophysics, Chinese Academy of Sciences https://orcid.org/0000-0001-5812-7221
Yanying Wang
Institute of Biophysics, Chinese Academy of Sciences
Zhen Xiong
Institute of Biophysics, Chinese Academy of Sciences
Dongdong Fan
Institute of Biophysics
Hui Guo
Chinese Academy of Sciences
Ying Du
Institute of Biophysics, Chinese Academy of Sciences
Feng Liu
Institute of Zoology, Chinese Academy of Sciences https://orcid.org/0000-0003-3228-0943
Yong Tian
Institute of Biophysics, Chinese Academy of Sciences https://orcid.org/0000-0002-8790-1148

Article

Keywords: Intestinal stem cells, self renewal, gut microbiota, valeric acid, macrophage

Posted Date: April 12th, 2021

DOI: https://doi.org/10.21203/rs.3.rs-376640/v1

Valeric acid-5-HT-dependent macrophage activation drives intestinal stem cell self-renewal

Pingping Zhu[1, 2, 3, 7]*, Tiankun Lu[1, 2, 7], Jiayi Wu[1, 7], Xiaoxiao Zhu[4, 7], Benyu Liu[1], Yanying Wang[1], Zhen Xiong[1], Dongdong Fan[4], Hui Guo[1], Ying Du[1], Feng Liu[6], Yong Tian[4, 5*], Zusen Fan[1, 5*]

[1]CAS Key Laboratory of Infection and Immunity, CAS Center for Excellence in Biomacromolecules, Institute of Biophysics, Chinese Academy of Sciences, Beijing 100101, China

[2]School of Life Sciences, Zhengzhou University, Zhengzhou 450001, China

[3]State Key Laboratory of Esophageal Cancer Prevention & Treatment, Zhengzhou University, Zhengzhou, Henan Province 450052, PR China

[4]CAS Key Laboratory of RNA Biology; Institute of Biophysics, Chinese Academy of Sciences, Beijing 100101, China

[5]University of Chinese Academy of Sciences, Beijing 100049, China

[6]State Key Laboratory of Membrane Biology, Institute of Zoology, Chinese Academy of Sciences, Beijing 100101

[7]These authors contributed equally to this paper.

*Correspondence should be addressed to Z.F. (fanz@moon.ibp.ac.cn), Y.T. (ytian@ibp.ac.cn) and P. Z (zhup@zzu.edu.cn).

Running title:

Macrophage activation drives intestinal stem cell self-renewal

Abstract

Lgr5^{+} intestinal stem cells reside within specialized niches at the crypt base and harbor self-renewal and differentiation capacities. ISCs in the crypt base are sustained by their surrounding niche for precise modulation of self-renewal and differentiation. However, how intestinal cells in the crypt niche and microbiota in enteric cavity regulates ISC stemness remains unclear. Here we show that ISCs are regulated by intestinal nerve cells and macrophage cells in the crypt niche, which are further modulated by microbiota. Enteric serotonergic neurons, along with their secreted neurotransmitter 5-HT, are required for ISC self-renewal. 5-HT activates PGE2 production in macrophages through engagement with its receptors Htr2a/3a, and PGE2 activates Wnt/β-catenin signaling of ISCs via engagement with its receptors Ep1/Ep4. Gut bacterial metabolite valeric acid promotes Tph2 expression through blocking enrichment of NuRD complex onto *Tph2* promoter. Our findings reveal the complicated crosstalk between microbiota, intestinal nerve cells, intestinal immune cells and intestinal stem cells, adding a new layer for ISC regulation by niche cells and microbiota.

Key words:

Intestinal stem cells; self-renewal; gut microbiota; valeric acid; macrophage

Introduction

Intestine is the largest digestive and absorptive organ, consisting of intestinal epithelium and lamina propria. Intestine epithelium, the most frequently renewing organ in adult mammals, contains five kinds of mature cells, including enterocytes, goblet cells, enteroendocrine cells, Paneth cells and tuft cells[1]. All these mature cells are derived from $Lgr5^+$ intestinal stem cells (ISCs), which reside at the crypt base and harbor self-renewal and differentiation capacities [2]. Many signaling pathways participate in the regulation of self-renewal and multipotency of $Lgr5^+$ ISCs, including Wnt/β-catenin signaling, Notch signaling, BMP signaling, ErbB signaling and Hedgehog signaling[3]. The self-renewal of ISCs is under precise regulation by numerous intracellular and extracellular signals. Recently, we identified an ISC-intrinsic long noncoding RNA lncGata6 was required for ISC self-renewal [4]. The extracellular niche provides Wnt, Notch and epidermal growth factor (EGF) signals to support ISC self-renewal and normal epithelial maintenance [5,6]. Numerous kinds of cells have been identified as niche cells for ISCs. In the small intestine, ISCs are interspersed between Paneth cells, which secrete critical molecules such as Wnt3, EGF, Notch, lactate and cyclic ADP ribose to maintain the stemness of ISCs [6-8]. Stroma cells and $FOXL1^+$ subepithelial telocytes and $CD90^+CD81^+CD34^+CD138^-$ MRISC also provide Wnt and Rspo ligands as ISC niche cells[9,10]. However, it is still elusive to define ISC niche cells and niche factors.

The ISC niche contains two major components: extracellular matrix (ECM) and cellular microenvironment. The cellular microenvironment comprises all the resident cells embedded within the ECM, including pericryptal myofibroblasts, fibroblasts, pericytes, endothelial cells, immune cells, neural cells, and smooth muscle cells. These cells secrete a wide range of matrix components and growth factors for the regulation of ISC self-renewal and differentiation[11,12]. Accumulating evidences demonstrate the critical role of immune cells in ISC self-renewal. For example, T cells from allogeneic transplantation mainly locate in ISC compartment and kill ISCs, which expressed MHC classes I and II molecules[13]. IL-22 secreted by group 3 ILCs (ILC3s) can promote ISC-mediated epithelial regeneration after intestinal damage, and drive ISC self-renewal [14,15]. Recently, we revealed that ILC2 cells promote ISC self-renewal through IL-13 pathway[16]. However, the

immunological mechanisms of ISCs remain largely unknown.

Beside immune cells, the intestinal tract contains an intrinsic nervous system that is termed as the enteric nervous system (ENS). The total number of enteric neurons is 400-600 million in human and almost equal to the number of neurons in spinal cord[17]. The ENS regulates the behavior of the gut and connects to the central nervous system (CNS)[18]. However, it remains unclear whether nerve cells, the extremely enriched cells in intestines, can support ISC self-renewal. 5-hydroxytryptamine (5-HT), also known as serotonin, plays important roles in enteric neurotransmission, initiation and propagation of intrinsic enteric reflexes, gut-to-brain connections, and many other biological processes[19]. Within the gut, 5-HT is synthesized by two types of cells, enterochromaffin (EC) cells and enteric serotonergic neurons of the myenteric plexus. The EC cells express tryptophan hydroxylase-1 (Tph1) to synthesize 5-HT and enteric serotonergic neurons express Tph2 to produce 5-HT[20]. 5-HT exerts its roles through engagement of 5-HT receptors. At least 14 members of 5-HT receptors have been identified up to date [21]. Most members of 5-HT receptors belong to the G-protein-coupled receptor (GPCR) superfamily, and only 5-HT3 receptor belongs to the ligand-gated ion channel. Different cell types harbor restricted receptors to receive 5-HT stimulation. For instance, Htr2b is highly expressed in white adipocytes and hepatocytes, and promotes lipolysis and liver gluconeogenesis during fasting [22]. Htr3a is highly expressed in brown adipocytes and pancreatic β cells, and participates in systemic energy homeostasis, brown adipose tissue thermogenesis and glucose-stimulated insulin secretion [23].

Intestinal epithelium is exposed to astounding numbers and diversity of microorganisms in the enteric cavity, collectively called gut microbiota[24]. The gut microbiota interacts with the host extensively and regulates various physiological and pathological processes. For example, the gut microbiota can regulate innate and adaptive immunological players, including epithelial cells, antigen-presenting cells, innate lymphoid cells and regulatory T cells[25]. The gut microbiota is also implicated in tumor initiation, progression and dissemination, as well as the response to cancer therapy[26]. In addition, germ-free (GF) mice show a reduced epithelial cell turnover rate owing to declined proliferation of intestinal epithelial cells and declined crypt-to-tip cellular migration [27],

suggesting the gut microbiota is involved in the modulation of intestine homeostasis. Here we show that gut microbiota metabolite valeric acid (VA) promotes 5-HT production in enteric serotonergic neurons and 5-HT signaling is required for the production of PGE2 in macrophages. PGE2 drives ISC self-renewal via engagement with its receptors Ep1/Ep4.

Results

Neurotransmitter 5-HT drives self-renewal of ISCs

To investigate the role of intestinal nerve cells in the regulation of ISC self-renewal, we treated *Lgr5*^{GFP} reporter mice with commercial neurotransmitter antagonists and counted *Lgr5*$^{GFP+}$ ISCs in intestine tissues after 3 days. We found that the 5-HT antagonist pCPA most significantly decreased the ratios of ISCs both in small intestines and colons (Figure 1A, B). In addition, pCPA treatment displayed decreased depth of crypts in small intestines and colons, and shrink of villi (Figure 1C). These observations were further confirmed by probing Lgr5 *in situ* hybridization (Figure 1D). Given the critical role of ISCs in intestinal regeneration after radiation damage [28], we then performed radiation damage with pCPA treatment and detected intestinal regeneration. As expected, pCPA treatment substantially inhibited intestinal regeneration and repair (Figure 1E). These data indicate that 5-HT plays a critical role in the maintenance of ISCs.

The serotonin transporter (SERT) can recycle 5-HT to terminate its action, and *Sert* deficient mice increased 5-HT. We found that *Sert* KO mice increased length of villi and crypts (Supplementary Figure 1A-C). In addition, *Sert* KO also increased ISC numbers both in small intestines and colons (Figure 1F). To further perform lineage tracing, *LR*^{lacZ};*Sert*$^{-/-}$ mice were established by crossing *Sert* KO mice with *Lgr5*$^{GFP\text{-}CreERT2}$ and *Rosa26*$^{lsl\text{-}lacZ}$ mice. We observed that *Sert* deletion increased ISC numbers and intestinal renewal ability (Figure 1G, H, and Supplementary Figure 1D). Altogether, 5-HT is required for the self-renewal maintenance of ISCs.

5-HT produced by enteric serotonergic neurons is required for ISC self-renewal

Within the gut, 5-HT is generated by enterochromaffin (EC) cells and enteric serotonergic neurons of myenteric plexus. The EC cells contain tryptophan hydroxylase-1 (Tph1) to be responsible for biosynthesis of 5-HT, whereas enteric serotonergic neurons express Tph2 for 5-HT production [29]. To determine the source cells for 5-HT production,

we generated *Tph1* KO mice and obtained *Tph2* KO mice (Supplementary Figure 2A-C). We found that *Tph2* KO mice displayed much shorter crypts and villi and reduced numbers of ISCs, whereas *Tph1* KO mice showed normal ISCs compared to littermate wild type (WT) mice (Figure 2A and Supplementary Figure 2D). These observations were further validated by staining another ISC marker Olfm4 and proliferation marker Ki67 antigen (Figure 2B, C). Moreover, *Tph2* KO mice also impaired intestinal regeneration post radiation damage (Figure 2D).

To further verify the role of EC cells and enteric serotonergic neurons in ISC self-renewal, we generated *Tph1*^{DTR} and *Tph2*^{DTR} mice through CRISPR/Cas9 approaches, in which EC cells and enteric serotonergic neurons will be depleted upon diphtheria toxin (DT) treatment (Supplementary Figure 2E, F). As expected, decreased ISC numbers and impaired ISC function could be observed in DT treated *Tph2*^{DTR} mice, whereas DT treated *Tph1*^{DTR} mice had normal ISC number and normal function compared to *Lgr5*^{GFP} mice (Figure 2E, F). These observations confirm that enteric serotonergic neurons play a critical role in ISC self-renewal and intestinal regeneration. Taken together, enteric serotonergic neurons are required for ISC self-renewal and intestinal regeneration.

5-HT activates Ptges expression in macrophages

We next explored the molecule mechanism of 5-HT in ISC self-renewal. First, we established organoid formation assay with ISC, crypt or ISC plus CD45$^+$ cells, and found 5-HT mainly activated ISC self-renewal through CD45$^+$ cells (Figure 3A, B). Among top10 lowly expressed genes in Tph2 KO CD45$^+$ cells, Ptges, a critical gene for PGE2 expression, was required for CD45$^+$ cells dependent ISC self-renewal (Figure 3C, D). Of note, *Ptges* KO mice showed decreased numbers of ISCs both in small intestines and colons (Figure 3E and Supplementary Figure 3A, B). Moreover, pCPA treatment impaired ISC function in WT ISCs, but not in *Ptges* KO ISCs, indicating an essential role of Ptges in 5-HT-mediated ISC self-renewal and function (Figure 3E).

Ptges was widely expressed in CD45$^+$ immune cells, and especially macrophages, which were regulated in 5-HT dependent Ptges expression (Figure 3F). Indeed, macrophage depletion largely decreased ISC numbers both in small intestines and colons (Figure 3G). Adoptive transfer of WT macrophages, but not *Ptges*$^{-/-}$ macrophages, was

able to rescue ISC numbers in Tph2 depletion mice (Figure 3H), indicating that 5-HT exerts its role in ISC self-renewal mainly through Ptges in macrophages. Similarly, 5-HT promoted ISC self-renewal via Ptges-dependent macrophage activation (Figure 3I). Collectively, 5-HT activates Ptges expression in macrophages.

5-HT promotes Ptges expression via engagement with its receptors Htr2a and Htr3a

5-HT exerts its role through its cognitive receptors, so we next detected the expression patterns of 5-HT receptors on macrophages. We silenced each receptor in macrophages and detected the role of 5-HT in Ptges expression. We noticed that Htr2a or Htr3a knockdown decreased Ptges expression, whereas knockdown of other 5-HT receptors had no significant inhibition (Figure 4A). Indeed, Htr2a and Htr3a were highly expressed in macrophages (Figure 4B). Moreover, blockade of Htr2a and Htr3a with their inhibitors Ketanserin and Tropisetron suppressed 5-HT-dependent PGE2 production (Figure 4C). We then generated *Htr2a* and *Htr3a* KO mice, and established double KO (DKO) mice by crossing these KO mice (Supplementary Figure 4A-D). Decreased PGE2 release was observed in *Htr2a* and *Htr3a* KO macrophages (Figure 4D). These data suggest that Htr2a and Htr3a are required for 5-HT- dependent PGE2 production. More importantly, *Htr2a* and *Htr3a* KO mice showed decreased numbers of ISCs, indicating the essential role of Htr2a and Htr3a in ISC maintenance (Figure 4E).

We then detected PGE2 function in ISC self-renewal. PGE2 treatment increased ISC numbers, whereas PGE2 inhibitor indomethacin treatment decreased ISC numbers (Figure 4F, G). In addition, PGE2 treatment promoted organoid formation of ISCs (Figure 4H), suggesting a critical role of PGE2 in ISC self-renewal. Finally, we observed that 5-HT activated NF-kB signaling pathway to initiate Ptges expression (Figure 4I-K, and Supplementary Figure 4E). Altogether, 5-HT activates PGE2 production through its cognitive receptors Htr2a and Htr3a on macrophages.

PGE2 promotes ISC self-renewal through Wnt/β-catenin signaling

The mechanism of PGE2 in ISC self-renewal is not clear. We silenced all the four PGE2 receptors for in vitro organoids formation assays. We found that knockdown of Ep1 or Ep4 was remarkably suppressed organoids formation (Figure 5A). We next generated Ep1 and Ep4 knockout mice, and these mice displayed much shorter crypts and villi, and

DKO mice showed much shorter crypts and villi than each single KO mice (Figure 5B and Supplementary Figure 5A-D). Expectedly, *Ep1*, *Ep4* KO mice and DKO mice decreased ISC numbers (Figure 5C, D). These results indicate that PGE2 signaling mediated by Ep1 and Ep4 is required for the ISC maintenance. In addition, DKO mice displayed impaired intestinal regeneration after radiation damage (Figure 5E). Reduced ISC stemness was further validated by lineage tracing assays (Figure 5F). Collectively, PGE2 signaling is initiated by engagement with its receptors Ep1 and Ep4 to maintain ISC stemness.

Considering the cross-talk between PGE2 and Wnt/β-catenin signaling, we next detected Wnt/β-catenin activation. We noticed that DKO ISCs inhibited Wnt/β-catenin signaling activation (Figure 5G, and Supplementary Figure 5E, F). In addition, we crossed DKO mice with *Axin2*^{lacZ} mice and found that DKO ISCs displayed impaired Wnt/β-catenin activation (Figure 5H). These data indicate that PGE2 signaling promotes β-catenin stability to initiate Wnt/β-catenin signaling activation. Taken together, PGE2 promotes ISC self-renewal through Wnt/β-catenin signaling.

Microbiota promotes Tph2 expression to generate 5-HT

It has been reported that the expression of Tph1 in EC cells is regulated by microbiota [30]. We wanted to explore whether the expression of Tph2 in enteric serotonergic neurons was also regulated by microbiota. Mice treated with ampicillin, neomycin and vancomycin (ABX) can destroy microbiota. We observed that ABX treated mice and Germ-free (GF) mice substantially impaired Tph2 expression (Figure 6A and Supplementary Figure 6A). Fecal microbiota transplantation (FMT) is able to restore normal microbiota in GF mice[31]. We found that FMT into GF mice restored the expression of Tph2 (Figure 6A). Of note, GF mice remarkably suppressed 5-HT production in myenteric plexus, whereas FMT into GF mice restored 5-HT generation (Supplementary Figure 6B). Through lineage tracing, we observed that ABX treatment and GF mice dramatically suppressed ISC stemness, whereas FMT treatment into GF mice restored the self-renewal capacity of ISCs (Figure 6B, C, and Supplementary Figure 6C). These results suggest that microbiota can regulate Tph2-mediated 5-HT generation to promote stemness of ISCs.

For many cases, microbiota secretes metabolites to participate in the regulation of biological processes[32]. We then used absorbable metabolites to treat GF mice and examined Tph2 expression levels in intestinal tissues [33]. Of these metabolites we examined, valeric acid (VA) could dramatically promote Thp2 expression in GF mice, while other metabolites we used had no such effect (Figure 6D). Tph2 expression enhanced by VA was further validated through immunohistochemistry and immunoblotting (Figure 6E and Supplementary Figure 6D). In addition, VA could promote expression of Wnt/β-catenin downstream genes in GF intestine (Figure 6E). Moreover, VA treatment was able to enhance 5-HT generation in GF myenteric plexus (Figure 6F). Consequently, VA treatment could augment Wnt/β-catenin signaling activation and restore the ISC numbers in GF intestine compared to SPF mice (Figure 6G, H). By contrast, VA treatment failed to promote Wnt/β-catenin signaling activation and restore the ISC numbers in *Tph2* deleted GF mice (Figure 6G, H), suggesting VA promotes ISC self-renewal in a Tph2-dependent manner. Similarly, ABX inhibited ISC self-renewal and Wnt/β-catenin activation via Tph2 (Supplementary Figure 6E, F). Collectively, VA secreted by microbiota promotes Tph2 expression and 5-HT-mediated ISC self-renewal.

VA inhibits enrichment of the NuRD complex onto *Thp2* promoter to initiate its expression

To further explore the molecular mechanism of microbiota-mediated Tph2 expression, we isolated myenteric plexus cells from GF mice and SPF mice, and examined chromatin accessibility of *Tph2* promoter by DNase sensibility assay. We found that the -3600~-3400 region of *Tph2* promoter was resistant to DNase digestion in GF mice, suggesting the *Tph2* promoter is suppressed in GF mice (Supplementary Figure 7A). The activation of *Tph2* promoter by VA was validated by luciferase assay (Supplementary Figure 7B). Hdac1, Hdac2 and Mbd3 were identified as protein candidates to bind *Tph2* promoter in GF cells through CAPTURE assay (Capture of Chromatin Interactions by Biotinylated dCas9)[34] (Figure 7A, and Supplementary Figure 7C). Hdac1, Hdac2 and Mbd3 are main components of the NuRD complex, which inhibits gene transcription [35]. Enhanced interaction of *Tph2* promoter with these three components was confirmed by Western blot (Figure 7B). However, FMT and VA treatment blocked the interaction of

NuRD complex with *Tph2* promoter (Figure 7B). These observations were further confirmed by ChIP and FISH assays (Figure 7C, D). These data suggest that FMT and VA treatment can inhibit the enrichment of the NuRD complex onto *Tph2* promoter.

H3K5ac and H3K9ac are two histone H3 modifications that are removed by Hdac1/2 [36]. H3K4me3 is an active marker for gene transcription activation [37]. We found that FMT and VA treatment enriched H3K5ac, H3K9ac and H3K4me3 onto *Tph2* promoter region (Figure 7E). We then established *Hdac1*, *Hdac2* and *Mbd3* deleted myenteric plexus cells through CRISPR/Cas9 approach (Supplementary Figure 7D). We noticed that deletion of *Hdac1*, *Hdac2* and *Mbd3* enhanced Tph2 expression in myenteric plexus cells (Figure 7F, and Supplementary Figure 7D). *Mbd3* KO mice also showed increased Tph2 expression in myenteric plexus cells (Figure 7G, and Supplementary Figure 7E). We also deleted the NuRD complex-binding region of *Tph2* promoter (*Tph2P* KO). We found that *Tph2P* KO cells increased Tph2 expression (Figure 7H). In addition, Hdac1, Hdac2 and Mbd3 overexpression inhibited Tph2 expression, whereas had no inhibitory effects in *Tph2P* KO cells (Figure 7I). Altogether, VA inhibits enrichment of the NuRD complex onto *Tph2* promoter to initiate Tph2 expression.

Discussion

Under homeostatic conditions, the intestinal epithelium harbors remarkable self-renewal capacity that is driven by ISCs residing within specialized niches at the crypt base [38]. The self-renewal of ISCs is under precise regulation by various intracellular and extracellular signals. In this study, we showed that neurotransmitter 5-HT and PGE2 are required for the self-renewal maintenance of ISCs and intestinal regeneration. Macrophages serve as crypt niche cells, which activates Wnt/β-catenin signaling in ISCs through engagement with its receptors Ep1/Ep4. The metabolite VA produced by gut microbiota promotes Tph2 expression in the enteric serotonergic neurons through suppression of the NuRD complex. Our works revealed the cross-talk between microbiota, enteric neurons, immune cells and intestinal stem cells, adding new layers for intestinal homostastasis regulation.

The intestinal 5-HT is generated by two types of cells, EC cells and enteric serotonergic neurons of the myenteric plexus, respectively being synthesized by

rate-limiting enzymes Tph1 and Tph2 [29]. The 5-HT generated by the EC cells overflows to gastrointestinal lumen and blood. Overflowing 5-HT from the EC cells is taken up and concentrated in platelets as a sole source of blood 5-HT. It has been reported that the 5-HT generated by the enteric serotonergic neurons mediates fast and slow excitatory neurotransmission and regulates gastrointestinal motility [39]. However, how intestinal 5-HT regulates ISCs is still unknown. Herein we showed that *Tph2*$^{-/-}$ mice, but not *Tph1*$^{-/-}$ mice, impairs the self-renewal maintenance of ISCs and intestinal regeneration. Our results suggest that the 5-HT generated by the enteric serotonergic neurons is involved in the self-renewal maintenance of ISCs.

5-HT exerts its functions through engagement with 5-HT receptors, including 13 distinct heptahelical G-protein-coupled receptors (GPCRs) and one ligand-gated ion channel [21]. Besides 5-HT and its receptors are identified to exist both in the central and peripheral nervous system (CNS/PNS), they are also contained in non-neuronal tissues such as gut, cardiovascular system and blood. Here we found that Htr2a and Htr3a are highly expressed on macrophage and these receptors have a synergetic effect on 5-HT signaling-mediated PGE2 production. Upon 5-HT engages with Htr2a/3a, these engaged receptors activate Ptges expression, which induces PGE2 production. PGE2 further activates Wnt/β-catenin activation and ISC self-renewal through Ep1 and Ep4.

Intestinal macrophages play critical roles in intestinal development, homeostasis, regeneration, aging, pathogen infection as well as inflammation[40,41]. Intestinal macrophages are a kind of tissue resident macrophages, and their functions are also finely regulated by various tissue factors. Increasing evidence indicates the critical role of macrophages in intestinal stem cells. CSF1R blockade causes a decreased Lgr5^{+} ISCs and aberrant differentiation of intestinal epithelial cell lineages[42]. AhR ablation in intestinal macrophages also disturbs intestinal epithelium development[43]. Macrophages secrete hepatocyte growth factor (HGF) to promote ISC self-renewal and differentiation[44]. Here we reveal a novel mechanism of intestinal macrophages in ISC self-renewal. Intestinal macrophages serve as signal transmitting cells in a neuro-immune-stem cell regulatory circuit, and modulate ISC self-renewal by upstream enteric serotonergic neurons. Intestinal macrophages express Htr2a and Ttr3a, which are required for the initiation of

5-HT signaling from enteric serotonergic neurons. Engagement of 5-HT with its receptors Htr2a/3a in intestinal macrophages promote Ptges expression and PGE2 release, which drives the self-renewal of ISCs via Wnt/β-catenin pathway. Besides intestinal macrophages, some 5-HT receptors are also expressed in intestinal epithelial cells[45], whose exact roles in the self-renewal of ISCs still need to be further investigated.

Gut microbiota plays critical roles in host health and disease, whose modulations mainly depend on direct stimulation of bacterial cell components and the effects of bacterial metabolites[46]. The bacterial cell components affect the physiological and pathological functions of the immune system via the direct stimulation of Toll-like receptors (TLRs) expressed by dendritic cells and colonocytes in the colonic mucosa [47]. Only a few of bacterial metabolites such as short-chain fatty acids (SCFA) have been defined [48], most of them are not well known yet. A recent report showed that many bacterial metabolites can be absorbed by colonocytes and somatic blood [33], indicating the critical roles of bacterial metabolites in the regulation of host health and disease. Kaiko et al. reported that many bacterial metabolites suppress ISC self-renewal through organoid formation assay [49]. Here we showed that the gut microbiota and metabolite VA are required for ISC self-renewal and intestinal regeneration. Moreover, VA can inhibit enrichment of the NuRD complex onto *Tph2* promoter to initiate Tph2 expression, which promotes 5-HT production in enteric serotonergic neurons. In our study, we demonstrate that bacterial metabolite VA can induce ISC self-renewal by in vivo lineage tracing assay. These differences between Kaiko et al. and our findings suggest that specific bacterial metabolites may have different roles in the regulation of intestinal homeostasis and regeneration. Our work adds a new layer for ISC regulation by enteric nervous system, enteric immune cells and gut microbiota.

Materials and Methods

Antibodies and reagents

Anti-Olfm4 (Cat#14369), anti-EPCAM (Cat# 14452) and anti-E-Cadherin (Cat# 8437S) antibodies were from Cell Signaling Technology. Anti-GFP (Cat# ab183735), anti-Ki67 (Cat# ab15580), and anti-Digoxin (Cat# ab51949) antibodies were obtained

from Abcam. Anti-WGA (Cat# GTX01500) antibody was purchased from GeneTex. Anti-β-catenin (Cat# 610154) antibody was obtained from BD Biosciences. Anti-Krt20 (Cat# 17329-1-AP) antibody was purchased from Proteintech. HRP-conjugated secondary antibodies were from Sungene Biotech. Alexa-594, Alexa-488, and Alexa-647-conjugated anti-rabbit and anti-mouse secondary antibodies were purchased from Invitrogen. OpalTM 7-color fIHC kit (Cat# MEL797001KT) was from PerKinElmer. Polymer HRP detection kits were from GBI labs. N2 supplement and B27 supplement were from Invitrogen. Wnt3a, RSPO1, Noggin and EGF proteins were purchased from Peprotech. N2 and B27 were from Invitrogen. 4',6-diamidino-2-phenylindole (DAPI), N-acetylcysteine, Y27632 and hyaluronidase were from Sigma-Aldrich.

Generation of knockout mice by CRISPR/Cas9 technology

Sert$^{-/-}$, *Tph1*$^{-/-}$, *Htr2a*$^{-/-}$, *Htr3a*$^{-/-}$, *Ptges*$^{-/-}$, *Ptger1*$^{-/-}$, *Ptger4*$^{-/-}$, *Tph1*^{DTR} and *Tph2*^{DTR}mice were generated using CRISPR/Cas9 approaches as described [50]. Approximate 250 zygotes in C57BL/6 background were injected with corresponding sgRNAs (Supplementary Table 1) and subsequently transferred to the uterus of pseudo-pregnant ICR females, from which viable founder mice were obtained. *Tph2* KO mice were obtained from Feng Liu Lab. All mouse genotypes were verified by DNA sequencing. Other gene modified mouse strains were: *Rosa26*$^{lsl\text{-}Cas9}$ mice were purchased from the Jackson Laboratory. *Lgr5*$^{GFP\text{-}CreERT2}$ mice were obtained from Model Animal Research Center of Nanjing University. *Rosa26*^{YFP} mice were purchased from Shanghai Biomodel Organism Science & Technology Development Co.,Ltd. *Rosa26*^{lacZ} mice were from Shanghai Bioray Laboratory. *Axin2*^{lacZ} and *Apc*$^{min/+}$ mice were from Nanjing Biomedical Research Institute of Nanjing University. All the mouse strains were C57BL/6 background and maintained under specific pathogen-free conditions with approval by the Institutional Committee of Institute of Biophysics, Chinese Academy of Sciences. The study is compliant with all relevant ethical regulations regarding animal research. For tamoxifen (TAM) injection, 200 μl TAM in sunflower oil (10 μg/μl) was intraperitoneally injected into *Lgr5*^{CreERT2} mice at 60 days old.

All SPF mice, including wild-type C57BL/6, were bred and housed in a barrier facility accredited by the Institutional Committee of Institute of Biophysics, Chinese Academy of

Sciences. GF C57BL/6J mice were maintained in GF conditions in vinyl isolators in the animal facility of Institute of Laboratory Animal Science, Chinese Academy of Medical Sciences and were used according to protocols approved by the Institutional Committee of Institute of Biophysics, Chinese Academy of Sciences.

Tyramide signal amplification for fluorescence in situ hybridization

For multiple-color staining, OpalTM 7-color fIHC kit was used according to the manual. Briefly, intestine paraffin sections were sequentially stained with Anti-GFP, anti-Krt20, anti-Ki67, anti-OLFM4 and anti-E-Cad primary antibodies, and HRP-conjugated secondary antibodies. One of the six Opal reagents were used for staining, followed by microwave treatment and another round staining. Opal520, Opal540, Opal570, Opal620, Opal650, Opal690 dyes were used for staining. Samples were visualized using Vectra Automated Quantitative Pathology Imaging System (PerkinElmer).

Intestinal organoid culture and competitive organoid formation assay

For intestinal organoid culture, murine intestines were digested by 0.1% type I collagenase (Invitrogen), and further incubated in 1×TrypLE express (Life Technologies) supplemented with 0.8 kU/ml DNaseI (Roche) for single cell preparation. $Lgr5^{+}$ cells were sorted using FACS. Intestinal organoid medium was used as previously described with minor modifications [2]. Briefly, Dulbecco's modified Eagle's medium/F12 medium (Invitrogen) was supplemented with 20 ng/ml EGF (Peprotech), 100 ng/ml Noggin, N2 (Invitrogen), B27 (Invitrogen), 1.25 mM N-acetylcysteine (Sigma-Aldrich), 1 mg/ml Rspo1 (peprotech), 20 mM Y27632 (Sigma-Aldrich). Medium was replaced every 2 days and pictures of organoids were taken 1 weeks later. For competitive organoid formation, 1×10^4 shCtrl ISCs from 60-day-old *Lgr5*^{GFP};*Rosa26*$^{lsl\text{-}lacZ}$ (*LR*^{lacZ}) mice were mixed with 1×10^4 *LR*^{YFP} shHtr ISCs, and incubated in organoid medium. 1 weeks later, organoids were collected for single cell preparation with 1×TrypLE, stained with APC-conjugated anti-YFP antibody, and analyzed by FACS for YFP. For organoid formation, ISCs were cultured in medium containing EGF, Rspo1, Noggin and 10 ng/ml 5-HT.

β-galactosidase staining for ISC tracing

For ISC tracing, 60-day-old *Lgr5*$^{GFP\text{-}IRES\text{-}CreERT2}$;*Rosa26*$^{lsl\text{-}lacZ}$ (*LR*^{lacZ}) mice were injected (i.p) with 2 mg tamoxifen in sunflower oil (10 μg/μl). On day 61, day 63, day 65

and day 90, 8 mice in one group were sacrificed and intestine tissues were obtained for β-galactosidase staining (Beyotime Biotechnology, Cat# RG0039). Briefly, intestines were incubated in fixation buffer (RG0039-1) at room temperature for 20 min and then washed with PBS. Samples were incubated in staining buffer (including 10 μl buffer A, 10 μl buffer B, 930 μl buffer C and 50 μl X-Gal) at 37℃ for 30 min, and the samples were then screened by EPSON ImageScanner III. Finally the traced units were counted.

Detection of β-catenin nuclear translocation

β-catenin nuclear translocation was performed through immunohistochemistry. Briefly, formalin-fixed intestinal sections were deparaffinized in xylene and then rehydrated in graded alcohols. After treated in 3% H_2O_2, the sections were boiled for antigen retrieval in 100°C citric acid buffer for 15 min, and then cooled down slowly. The sections were then incubated in anti-β-catenin antibody overnight, followed by HRP secondary antibody.

In situ hybridization and fluorescence in situ hybridization

For Lgr5 *in situ* hybridization, mouse *Lgr5* gene was cloned into PCDNA4 plasmid and *in situ* probes targeting 1 kb N-terminal fragment of mouse *Lgr5* were labeled with Digoxin through in vitro transcription. Intestinal sections were rehydrated, treated with 0.2 M HCl and proteinase K solution, and then incubated in acetic anhydride solution, followed by hybridization overnight at 68°C with *Lgr5* probes in hybridization buffer (5× standard saline citrate (SSC; pH 4.5), 2% blocking powder (Roche), 50 μg/mL yeast transfer RNA, 50% formamide, 5 mmol/L ethylenediaminetetraacetic acid, 0.05% 3[3-cholaminopropyl diethylammonio]-1-propane sulfonate, 50 μg/mL heparinm 0.1% Tween 20). Samples were then rinsed in 2× SSC and washed with 2× SSC/50% formamide at 60°C for 3 × 20 min. Then sections were blocked for 30 min in TBST containing 0.5% blocking powder (Roche), followed by overnight's incubation at 4°C in blocking solution with HRP-conjugated anti-digoxigenin (1:2000 dilution; Roche).

CRISPR affinity purification in situ of regulatory elements

CRISPR affinity purification in situ of regulatory elements (CAPTURE) assay was performed to as described[34]. Briefly, pEF1a-BirA-V5-neo (addgene no. 100548)

pEF1a-FB-dCas9-puro (addgene no. 100547) and Tph2 promoter were overexpressed for intracellular dCas9 biotinylation and purified with Streptavidin, and the enrichment of Tph2 promoter binding proteins were identified through silver staining and Mass spectrum, and confirmed by Western blot.

***Tph2* promoter knockout**

Myenteric plexus cells were isolated from *Rosa26*$^{lsl\text{-}Cas9\text{-}GFP}$ mice and treated by two sgRNAs targeting -3600~-3500 region of *Tph2* promoter, followed by monoclonalization in neurosphere formation medium. *Tph2* promoter deleted neurospheres were detected by agarose gel electrophoresis and confirmed by DNA sequencing, and finally five neurospheres were established. Neurospheres were differentiated and Tph2 expression was examined by confocal microscopy. Myenteric plexus isolation, neurosphere formation and differentiation assays were performed as previously described [51].

Western blot

ISCs or myenteric plexus cells were crushed with RIPA buffer (150 mM NaCl, 0.1% SDS, 1% NP40, 0.5% sodium deoxycholate, 1 mM EDTA, 50 mM Tris, pH 8.0) and separated with SDS-PAGE. Then samples were then transferred to NC membrane (Beyotime Biotechnology, Shanghai, China) and incubated with primary antibodies. After washing with TBST three times, membranes were incubated with HRP-conjugated secondary antibodies for visualization [52].

Chromatin immunoprecipitation (ChIP)

ChIP was performed according to the standard protocol (Upstate Biotechnology, Inc.). Briefly, myenteric plexus cells were fixed in 1% formaldehyde for 10 min at 37 °C, and then cracked by SDS lysis buffer for 10 min on ice, followed by ultrasonic to shear DNA into fragments between 200 and 500 bp. Anti-Hdac1, anti-Hdac2, anti-H4K5ac, anti-H3K9ac and anti-H3K4me3 antibodies were used for ChIP assays as described [53].

TOPFLash

TOPFlash assay was used for Wnt/β-catenin activation detection. TOPFlash (Plasmid #12456, Addgene) and FOPFlash (Plasmid #12457, Addgene) were transfected into ISCs ($1x10^5$) along with thymidine kinase (TK) through electroporation, followed by 36 h incubation in organoid formation medium. Then cells were lyzed and detected using

substrates L and S (Promega dual luciferase kit). Wnt/β-catenin activation was measured by fold changes of TOPFlash versus FOPFlash as control.

Realtime PCR

Total RNA was extracted from ISCs or myenteric plexus cells, and used for reverse transcription PCR (RT-PCR). Complement DNA (cDNA) was used as templates for realtime PCR. Sequence specific primers for detected genes were listed in the Supplementary Table 2.

Co-immunoprecipitation (co-IP) assay

For co-IP, samples were lyzed with RIPA buffer for 30 min at 4 °C and precipitation was removed from cell lysates by centrifugation (12000g×10min). Supernatants were pre-cleared by protein A/G beads (Santa Cruz Biotechnology) for 1 h, and anti-Htr1b, anti-Axin1 or anti-β-catenin antibody was added for 4 h incubation. New protein A/G beads were added for immunoprecipitation. Precipitates were collected and examined by Western blot with indicated antibodies.

Statistics and reproducibility

For statistical evaluation, an unpaired Student's *t*-test was applied for calculating statistical probabilities in this study. For all panels, at least three independent experiments were performed with similar results, and representative experiments are shown. Data were analyzed by GraphPad Prism 5.0. Kaplan–Meier survival analysis was performed by SPSS 20.0. All flow cytometry data were analyzed with FlowJo 10 (Treestar). Adobe Photoshop CC 14.0 and ImageJ 1.48 were used for figure presentation. One-tailed unpaired Student's *t*-test was performed using Excel 2010. *P*-values ≤0.05 were considered significant (*, $P<0.05$; **, $P<0.01$; ***, $P<0.001$); $P>0.05$, non-significant (NS).

Data availability

All other data supporting the findings of this study are available from the corresponding author on reasonable request.

Acknowledgements

We thank Drs. Yihui Xu and Yan Teng for technical support. We thank Xiang Shi, Na Li, Shu Meng, Jing Cheng and Xing Gao for providing GF and SPF facilities. We thank

Jing Li (Cnkingbio Company Ltd, Beijing, China) for technical support. This work was supported by the Ministry of Science and Technology of China (2020YFA0803501, 2019YFA0508501), National Natural Science Foundation of China (31930036, 31922024, 81921003, 92042302, 91940305, 31771638), Strategic Priority Research Programs of the Chinese Academy of Sciences (XDB19030203).

Author contributions

P.Z. designed and performed experiments, analyzed data and wrote the paper; J.W., and L.H. performed experiments and analyzed data; X.Z. and D.F. generated genome modified mice; F.L. provided *Tph2* KO mice; B.L., Y.W., Z.X., H.G. and Y.D. performed some experiments; Y.T. initiated and analyzed data; Z.F. initiated the study, organized, designed, and wrote the paper.

Conflict of interest disclosure

The authors declare no competing financial interests.

References

1 Gehart, H. & Clevers, H. Tales from the crypt: new insights into intestinal stem cells. *Nat Rev Gastro Hepat* **16**, 19-34 (2019).

2 Sato, T. *et al.* Single Lgr5 stem cells build crypt-villus structures in vitro without a mesenchymal niche. *Nature* **459**, 262-U147 (2009).

3 Hu, D., Yan, H., He, X. C. & Li, L. Recent advances in understanding intestinal stem cell regulation. *F1000Research* **8** (2019).

4 Zhu, P. P. *et al.* LncGata6 maintains stemness of intestinal stem cells and promotes intestinal tumorigenesis. *Nat Cell Biol* **20**, 1134-1145 (2018).

5 Barker, N. *et al.* Identification of stem cells in small intestine and colon by marker gene Lgr5. *Nature* **449**, 1003-U1001 (2007).

6 Sato, T. *et al.* Paneth cells constitute the niche for Lgr5 stem cells in intestinal crypts. *Nature* **469**, 415-418 (2011).

7 Rodriguez-Colman, M. J. *et al.* Interplay between metabolic identities in the intestinal crypt supports stem cell function. *Nature* **543**, 424-435 (2017).

8 Yilmaz, O. H. *et al.* mTORC1 in the Paneth cell niche couples intestinal stem-cell function to calorie intake. *Nature* **486**, 490-U487 (2012).

9 Shoshkes-Carmel, M. *et al.* Subepithelial telocytes are an important source of Wnts that supports intestinal crypts. *Nature* **557**, 242-254 (2018).

10 Wu, N. *et al.* MAP3K2-regulated intestinal stromal cells define a distinct stem cell niche. *Nature*, doi:10.1038/s41586-021-03283-y (2021).

11 McCarthy, N., Kraiczy, J. & Shivdasani, R. A. Cellular and molecular architecture of the intestinal stem cell

niche. *Nat Cell Biol* **22**, 1033-1041 (2020).

12 Santos, A. J. M., Lo, Y. H., Mah, A. T. & Kuo, C. J. The Intestinal Stem Cell Niche: Homeostasis and Adaptations. *Trends Cell Biol* **28**, 1062-1078 (2018).

13 Fu, Y. Y. *et al.* T Cell Recruitment to the Intestinal Stem Cell Compartment Drives Immune-Mediated Intestinal Damage after Allogeneic Transplantation. *Immunity* **51**, 90-102 (2019).

14 Lindemans, C. A. *et al.* Interleukin-22 promotes intestinal-stem-cell-mediated epithelial regeneration. *Nature* **528**, 560-564 (2015).

15 Lindemans, C. A. *et al.* Interleukin-22 promotes intestinal-stem-cell-mediated epithelial regeneration. *Nature* **528**, 560-565 (2015).

16 Zhu, P. *et al.* IL-13 secreted by ILC2s promotes the self-renewal of intestinal stem cells through circular RNA circPan3. *Nat Immunol* **20**, 183–194 (2019).

17 Spencer, N. J. & Hu, H. Z. Enteric nervous system: sensory transduction, neural circuits and gastrointestinal motility. *Nat Rev Gastro Hepat* **17**, 338-351 (2020).

18 Margolis, K. G., Cryan, J. F. & Mayer, E. A. The Microbiota-Gut-Brain Axis: From Motility to Mood. *Gastroenterology* (2021).

19 Sahu, A. *et al.* The 5-Hydroxytryptamine signaling map: an overview of serotonin-serotonin receptor mediated signaling network. *J Cell Commun Signal* **12**, 731-735, (2018).

20 Gutknecht, L., Kriegebaum, C., Waider, J., Schmitt, A. & Lesch, K. P. Spatio-temporal expression of tryptophan hydroxylase isoforms in murine and human brain: convergent data from Tph2 knockout mice. *Eur Neuropsychopharm* **19**, 266-282 (2009).

21 Hoyer, D., Hannon, J. P. & Martin, G. R. Molecular, pharmacological and functional diversity of 5-HT receptors. *Pharmacol Biochem Be* **71**, 533-554 (2002).

22 Sumara, G., Sumara, O., Kim, J. K. & Karsenty, G. Gut-Derived Serotonin Is a Multifunctional Determinant to Fasting Adaptation. *Cell Metab* **16**, 588-600 (2012).

23 Crane, J. D. *et al.* Inhibiting peripheral serotonin synthesis reduces obesity and metabolic dysfunction by promoting brown adipose tissue thermogenesis. *Nat Med* **21**, 166-172 (2015).

24 Zmora, N., Suez, J. & Elinav, E. You are what you eat: diet, health and the gut microbiota. *Nat Rev Gastro Hepat* **16**, 35-56 (2019).

25 Jiao, Y. H., Wu, L., Huntington, N. D. & Zhang, X. Crosstalk Between Gut Microbiota and Innate Immunity and Its Implication in Autoimmune Diseases. *Front Immunol* **11** (2020).

26 Wong, S. H. & Yu, J. Gut microbiota in colorectal cancer: mechanisms of action and clinical applications. *Nat Rev Gastro Hepat* **16**, 690-704 (2019).

27 Sommer, F. & Backhed, F. The gut microbiota--masters of host development and physiology. *Nat Rev Microbiol* **11**, 227-238 (2013).

28 Metcalfe, C., Kljavin, N. M., Ybarra, R. & de Sauvage, F. J. Lgr5(+) Stem Cells Are Indispensable for Radiation-Induced Intestinal Regeneration. *Cell Stem Cell* **14**, 149-159 (2014).

29 Gershon, M. D. & Tack, J. The serotonin signaling system: From basic understanding to drug development-for functional GI disorders. *Gastroenterology* **132**, 397-414 (2007).

30 Yano, J. M. *et al.* Indigenous Bacteria from the Gut Microbiota Regulate Host Serotonin Biosynthesis (vol 161, pg 264, 2015). *Cell* **163**, 258-258 (2015).

31 Ooijevaar, R. E., Terveer, E. M., Verspaget, H. W., Kuijper, E. J. & Keller, J. J. Clinical Application and Potential of Fecal Microbiota Transplantation. *Annu Rev Med* **70**, 335-351 (2019).

32 Chen, H. W. *et al.* A Forward Chemical Genetic Screen Reveals Gut Microbiota Metabolites That Modulate Host Physiology. *Cell* **177**, 1217-1131 (2019).

33 Matsumoto, M. *et al.* Colonic Absorption of Low-Molecular-Weight Metabolites Influenced by the Intestinal Microbiome: A Pilot Study. *PloS one* **12**, e0169207 (2017).

34 Liu, X. *et al.* In Situ Capture of Chromatin Interactions by Biotinylated dCas9. *Cell* **170**, 1028-1043 (2017).

35 Zhang, Y. *et al.* Analysis of the NuRD subunits reveals a histone deacetylase core complex and a connection with DNA methylation. *Genes Dev* **13**, 1924-1935 (1999).

36 Ekwall, K. Genome-wide analysis of HDAC function. *Trends Genet* **21**, 608-615 (2005).

37 Benayoun, B. A. *et al.* H3K4me3 Breadth Is Linked to Cell Identity and Transcriptional Consistency. *Cell* **163**, 1281-U1264 (2015).

38 Barker, N. Adult intestinal stem cells: critical drivers of epithelial homeostasis and regeneration. *Nat Rev Mol Cell Bio* **15**, 19-33 (2014).

39 Sikander, A., Rana, S. V. & Prasad, K. K. Role of serotonin in gastrointestinal motility and irritable bowel syndrome. *Clin Chim Acta* **403**, 47-55 (2009).

40 De Schepper, S. *et al.* Self-Maintaining Gut Macrophages Are Essential for Intestinal Homeostasis (vol 175, pg 400, 2018). *Cell* **176**, 676-676 (2019).

41 Na, Y. R., Stakenborg, M., Seok, S. H. & Matteoli, G. Macrophages in intestinal inflammation and resolution: a potential therapeutic target in IBD. *Nat Rev Gastro Hepat* **16**, 531-543 (2019).

42 Sehgal, A. *et al.* The role of CSF1R-dependent macrophages in control of the intestinal stem-cell niche. *Nat Commun* **9** (2018).

43 Chng, S. H. *et al.* Ablating the aryl hydrocarbon receptor (AhR) in CD11c+ cells perturbs intestinal epithelium development and intestinal immunity. *Sci Rep* **6**, 23820 (2016).

44 D'Angelo, F. *et al.* Macrophages promote epithelial repair through hepatocyte growth factor secretion. *Clin Exp Immunol* **174**, 60-72 (2013).

45 Glatzle, J. *et al.* Expression of 5-HT3 receptors in the rat gastrointestinal tract. *Gastroenterology* **123**, 217-226 (2002).

46 Lavelle, A. & Sokol, H. Gut microbiota-derived metabolites as key actors in inflammatory bowel disease. *Nat Rev Gastro Hepat* **17**, 223-237 (2020).

47 Round, J. L. & Mazmanian, S. K. The gut microbiota shapes intestinal immune responses during health and disease (vol 9, pg 313, 2009). *Nat Rev Immunol* **9**, 600-600 (2009).

48 Kim, C. H., Park, J. & Kim, M. Gut microbiota-derived short-chain Fatty acids, T cells, and inflammation. *Immune netw* **14**, 277-288 (2014).

49 Kaiko, G. E. *et al.* The Colonic Crypt Protects Stem Cells from Microbiota-Derived Metabolites. *Cell* **167**, 1137 (2016).

50 Zhu, X. X. *et al.* An Efficient Genotyping Method for Genome-modified Animals and Human Cells Generated with CRISPR/Cas9 System. *Sci Rep-Uk* **4** (2014).

51 Grundmann, D., Klotz, M., Rabe, H., Glanemann, M. & Schafer, K. H. Isolation of high-purity myenteric plexus from adult human and mouse gastrointestinal tract. *Sci Rep* **5**, 9226 (2015).

52 Zhu, P. P. *et al.* LncBRM initiates YAP1 signalling activation to drive self-renewal of liver cancer stem cells. *Nat Commun* **7** (2016).

53 Zhu, P. P. *et al.* ZIC2-dependent OCT4 activation drives self-renewal of human liver cancer stem cells. *J Clin Invest* **125**, 3795-3808 (2015).

Figure legends

Figure 1. 5-HT drives self-renewal of ISCs. (A, B) 2-month old *Lgr5*^{GFP} mice were treated with indicated antagonists of neurotransmitters. Three days later, crypts of small intestine (A) and colon (B) were collected, and *Lgr5*$^{GFP+}$ ISCs were detected by FACS. Ratios of *Lgr5*$^{GFP+}$ ISCs in total crypt cells were shown as scatter diagram. *n*=8 *Lgr5*^{GFP} mice for each panel. (C) 2-month old mice were treated with 5-HT inhibitor pCPA for 36 h and 72 h, and representative H&E images of small intestine (SI) and colon were shown in left panel. *n*=50 fields from five mice were observed and shown in right panel. (D) Lgr5 *in situ* hybridization was performed in small intestine (SI) and colon tissues from pCPA treated mice. Typical images were shown in left panel, and statistical results of *n*=50 fields from five mice were in right panel. (E) pCPA treated mice were treated with 10 Gy's radiation, and sacrificed at indicated time points. Intestinal tissues were collected for H&E staining (upper panel). Numbers of intact crypts were shown in lower panel (means±s.d). Five 2-month old mice were used and *n*=20 fields were taken for each group. (F) *Sert* KO small intestine (SI) and colon crypts were collected for ISC detection by FACS. Ratios of *Lgr5*$^{GFP+}$ ISCs were shown. (G) *Lgr5*$^{GFP\text{-}CreERT2}$;*Rosa26*$^{lsl\text{-}lacZ}$ (*LR*^{lacZ}) mice were crossed with *Sert*$^{-/-}$ mice, followed by administration of tamoxifen (TAM) for lineage tracing analysis through intestinal whole-mount staining for β-gal. *n*=7 mice were sacrificed at indicated time points and typical jejunum sections on P65 (postnatal day 65) were shown. (H) *LR*^{lacZ};*Sert*$^{-/-}$ mice were used for lineage tracing analysis, and intestinal tissues were stained for lacZ observation. For C-E, scale bars, 100 μm. * $P < 0.05$, ** $P < 0.01$, *** $P < 0.001$ by unpaired one-tailed Student's *t*-test. At least three independent experiments were performed with similar results, and representative experiments were shown.

Figure 2. 5-HT generated by enteric serotonergic neurons contributes to ISC self-renewal. (A) Lgr5 *in situ* hybridization was performed in small intestine (SI) and colon tissues from *Tph1* and *Tph2* knockout mice. Typical image were shown in left panel, and *n*=50 fields from five mice were observed and shown in right panel. Scale bars, 100 μm. (B, C) *Lgr5*^{GFP};*Tph1*$^{-/-}$ mice and *Lgr5*^{GFP};*Tph2*$^{-/-}$ mice were sacrificed on P60 and intestine tissues were collected for immunofluorescence staining by indicated antibodies. Typical

images of small intestine (B) and large intestine (C) are shown. Scale bars, 50 μm. (D) *Tph1* and *Tph2* knockout mice were treated with 10 Gy's radiation, and sacrificed at indicated time points. Intestinal tissues were collected for H&E staining (upper panel) and numbers of intact crypts were shown in lower panel (means±s.d). *n*=20 fields from five mice were taken for each group. Scale bars, 100 μm. (E) Fluorescence staining of intestinal tissue from 2-month-old $Lgr5^{GFP}$, $Lgr5^{GFP}$;$Tph1^{DTR}$ and $Lgr5^{GFP}$;$Tph2^{DTR}$ mice 5 days after diphtheria toxin treatment. Scale bars, 50 μm. (F) LR^{lacZ};$Tph1^{DTR}$ and LR^{lacZ};$Tph2^{DTR}$ mice were used for lineage tracing analysis, and intestinal tissues were stained for lacZ observation. * $P < 0.05$, ** $P < 0.01$, *** $P < 0.001$ by unpaired one-tailed Student's *t*-test. At least three independent experiments were performed with similar results, and representative experiments were shown.

Figure 3. 5-HT activates Ptges expression in macrophages. (A, B) Organoid formation of ISC and crypt (A), or ISCs co-cultured with $CD45^+$ cells (B). Organoid formation medium was supplemented with/without 5-HT. (C) Heat map of Tph2 knockout and control propria cells, with top10 lowly expressed genes in Tph2 knockout cells listed in right. Red, high expression; Blue, low expression. (D) Organoid formation ratios of ISCs co-cultured with propria cells in which indicated genes were silenced individually. (E) ISC ratios of $Ptges^{+/+}$ and $Ptges^{-/-}$ mice, which were treated with pCPA 3 days before ISC detection. (F) Realtime PCR analysis for Ptges expression in indicated cells isolated from $Tph2^{+/+}$ and $Tph2^{-/-}$ mice. (G) Lgr5 *in situ* hybridization in small intestine (SI) and colon tissues of macrophage depleted mice, which were treated with CSF1R ab (antibody). Scale bars, 50 μm. (H) FACS detection for ISC ratios in small intestines (SI) and colon crypts from indicated treated mice. (I) Organoid formation of ISCs, co-cultured with WT or Ptges knockout macrophages. Typical images were in left panel and organoid formation ratios in right panels. At least three independent experiments were performed with similar results, and representative experiments were shown.

Figure 4. 5-HT promotes PGE2 expression with engagement with its receptors Htr2a and Htr3a. (A) Realtime PCR for Ptges expression levels in 5-HT treated macrophages,

in which the indicated 5-HT receptors were silenced individually. (B) High expression of Htr2a and Htr3a in intestinal macrophage cells, which were enriched via FACS. (C) PGE2 production in macrophages treated with indicated inhibitors of 5-HT receptor. (D) ELISA detection for PGE2 production in microphages, which were sorted from 5-HT treated Htr2a KO, Htr3a KO or DKO mice. All PGE2 levels were normalized to those of Vehicle treated mice. (E) Fluorescence staining of intestinal tissue from 2-month-old *Lgr5*^{GFP}, *Lgr5*^{GFP};*Ttr2a*$^{-/-}$, *Lgr5*^{GFP};*Ttr3a*$^{-/-}$ and *Lgr5*^{GFP};*Ttr2a*$^{-/-}$;*Ttr3a*$^{-/-}$ mice. (F, G) FACS detection for ISC ratios in small intestine (SI) or colon tissues from dmPGE2 treated (F) or indomethacin (Indo) treated (G) mice. (H) Organoid formation of ISCs, supplemented with/without PGE2. (I) Gene ontology analysis for pathway alterations in *Tph2*$^{+/+}$ and *Tph2*$^{-/-}$ cells. (J) ELISA detection for PGE2 production in indicated treated macrophages. (K) Realtime PCR analysis to detect enrichment of *Ptges* promoter (-3200~-3000 fragment) in ChIP eluate, using P65 antibody and indicated treated macrophages. At least three independent experiments were performed with similar results, and representative experiments were shown.

Figure 5. PGE2 drives Wnt signaling activation to maintain ISC stemness. (A) Orgnoid formation assay of indicated PGE2 receptor silenced ISCs, using PGE2 supplemented medium. (B) H&E staining of small intestine (SI) and colon of WT, *Ep1*$^{-/-}$, *Ep4*$^{-/-}$and DKO mice. Typical images were shown in left panel and *n*=50 fields were observed in right panel. Scale bars, 50 μm. (C) FACS detection for ISC ratios in small intestine (SI) and colon crypt, which were from WT, *Ep1*$^{-/-}$, *Ep4*$^{-/-}$and DKO mice. (D) Fluorescence staining of intestinal tissue from 2-month-old *Lgr5*^{GFP}, *Lgr5*^{GFP};*Ep1*$^{-/-}$, *Lgr5*^{GFP};*Ep4*$^{-/-}$ and *Lgr5*^{GFP};*Ep1*$^{-/-}$;*Ep4*$^{-/-}$ mice. Scale bars, 50 μm. (E) WT and DKO mice were treated with 10 Gy's radiation, and sacrificed at indicated time points, and typical images were shown. Scale bars, 100 μm. (F) *Lgr5*$^{GFP\text{-}CreERT2}$;*Rosa26*$^{lsl\text{-}lacZ}$ (*LR*^{lacZ}) mice were crossed with DKO mice, and intestinal whole-mount staining of β-gal was performed for lineage tracing analysis. *n*=8 mice were observed for each group and typical jejunum sections were shown. (G) Heatmap of indicated Wnt/β-catenin target genes in WT and DKO ISCs. (H) WT and DKO mice were crossed with *Axin2*^{lacZ} mice. Small intestinal (SI)

and colon tissues were stained for β-gal expression. β-gal staining indicates the activation of Wnt/β-catenin signaling. Scale bars, 50 μm. * $P < 0.05$, ** $P < 0.01$, *** $P < 0.001$ by unpaired one-tailed Student's *t*-test. At least three independent experiments were performed with similar results, and representative experiments were shown.

Figure 6. Microbiota promotes Tph2 expression to generate 5-HT. (A) SPF mice, GF mice and FMT into GF mice were used for Tph2 immunohistochemistry. Typical images of small intestine (SI) and colon tissues were shown. Scale bars, 100 μm. (B) *Lgr5*$^{GFP\text{-}CreERT2}$;*Rosa26*$^{lsl\text{-}lacZ}$ (*LR*^{lacZ}) mice in SPF, GF states, and FMT into GF mice were treated with tamoxifen (TAM) for lineage tracing analysis. 5 days later, GFP and lacZ signals were detected by confocal microscopy. Scale bars, 20 μm. (C) SPF, GF and FMT into GF *LR*^{lacZ} mice were treated with TAM for lineage tracing analysis. *n*=8 mice were sacrificed at indicated time points and typical jejunum sections on P65 were shown. Numbers of traced crypt-villus units (blue plots) at indicated time points were shown in lower panel (means±s.d). (D) GF mice were treaded with indicated metabolites, and Thp2 in intestine tissues was detected by realtime PCR. SPF and Ex-GF mice were used for positive controls. (E) Total intestine tissues from treated mice were lyzed for Western blot. β-actin was used as a loading control. (F) Myenteric plexus was isolated from treated mice, and 5-HT was detected by confocal microscopy. Typical images and 5-HT$^+$ ratios were shown. Scale bars, 50 μm. (G) Colon tissues from treated mice were used for realtime PCR analysis. ISC-related genes (*Olfm4, Ascl2*) and Wnt/β-catenin target genes (*c-Myc, Axin2, Ccnd2, Sox9*) were detected. (H) Colon tissues were obtained from VA treated mice and ISCs were detected by FACS. Ratios of ISCs were shown.* $P < 0.05$, ** $P < 0.01$, *** $P < 0.001$ by unpaired one-tailed Student's *t*-test. At least three independent experiments were performed with similar results, and representative experiments were shown.

Figure 7. VA inhibits enrichment of the NuRD complex onto *Thp2* promoter to initiate its expression. (A) Silver staining of eluate from CAPTURE assay (Capture of Chromatin Interactions by Biotinylated dCas9) using SPF, GF and VA treated cells.

Increased bands in GF cells were identified as Hdac1, Hdac2 and Mbd3. (B) The interaction of *Tph2* promoter with Hdac1, Hdac2 and Mbd3 in indicated myenteric plexus was detected by DNA pulldown and Western blot. (C) Indicated myenteric plexus cells were obtained for ChIP assay against Hdac1, Hdac2 and Mbd3. Enrichment of *Thp2* promoter was examined by realtime PCR. (D) Enteric serotonergic neurons were sorted by Tph2, and confirmed by 5-HT staining, followed by FISH for *Tph2* promoter detection and immunofluorescence staining for Hdac1. Co-localization of *Tph2* promoter with Hdac1 in enteric serotonergic neurons of GF mice was shown in left panel. Ratios of co-localized cells were shown in right panel. n=3 mice were used per panel, and 100 cells were observed per mouse. Scale bars, 4 μm. (E) H4K5ac, H3K9ac and H3K4me3 modifications of *Thp2* promoter were detected by ChIP assay. -3600~-3400 region of *Thp2* promoter were detected by realtime PCR. (F, G) *Hdac1*, *Hdac2* and *Mbd3* knockout cells were treated with VA, and Tph2 expression was detected by realtime PCR. (H) *Rosa26*$^{lsl\text{-}Cas9\text{-}GFP}$ mice were used for *Tph2* promoter knockout (*Tph2P* KO), and then Tph2 expression was measured by confocal microscopy. Five *Tph2P* KO clones were established. Typical neurosphere images were shown in left panel and Tph2^{+} cell ratios were shown in right panel. Scale bars, 10 μm. (I) *Tph2* promoter (*Tph2P*) knockout cells were treated with VA or overexpressed the NuRD components, followed by Tph2 expression. * $P < 0.05$, ** $P < 0.01$, *** $P < 0.001$ by unpaired one-tailed Student's t-test. At least three independent experiments were performed with similar results, and representative experiments were shown.

Figures

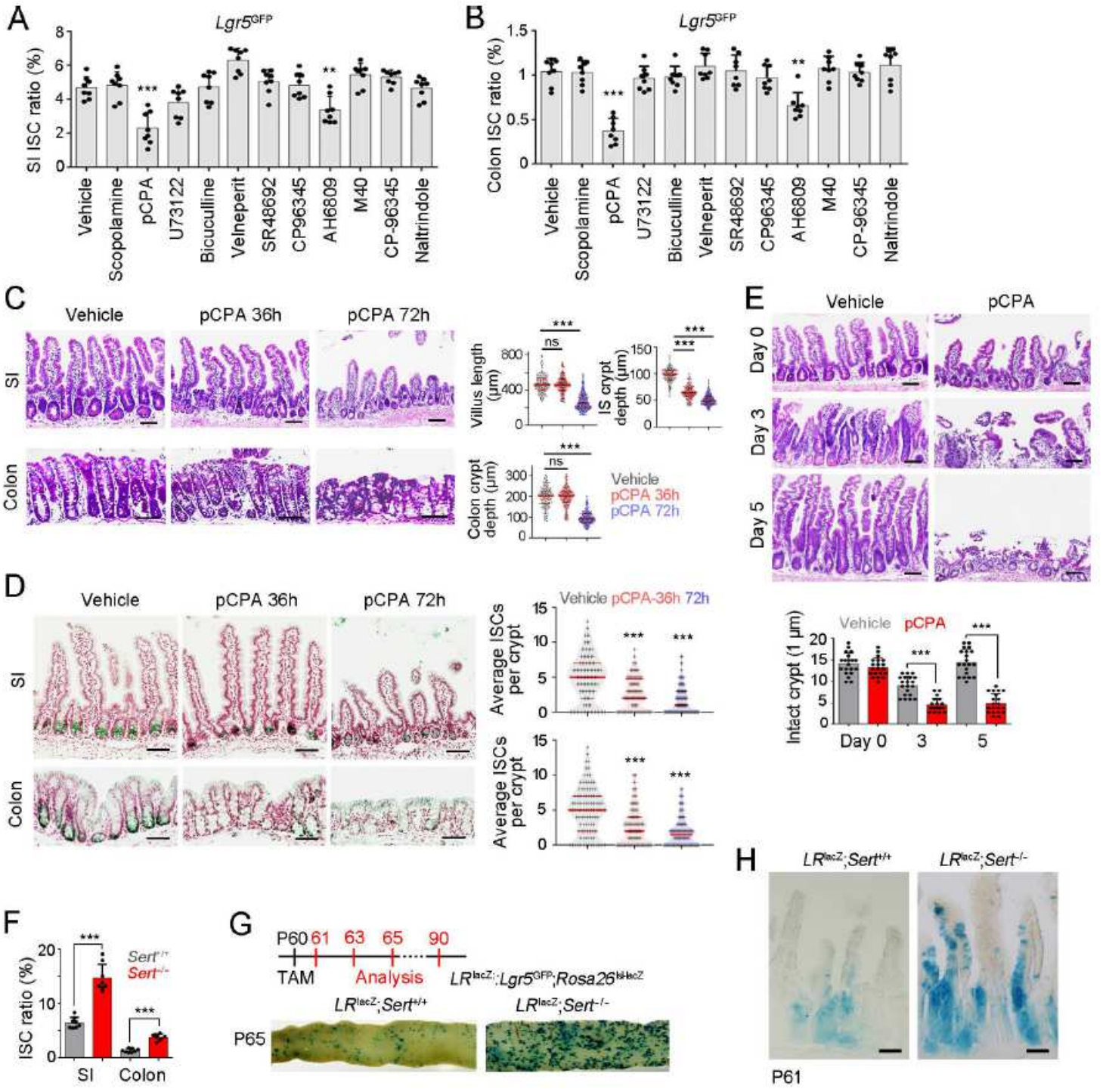

Figure 1

5 HT drives self renewal of ISC s . (A, B) 2 month old Lgr5 GFP mice were treated with indicated antagonists of neurotransmitters. Three days later, crypts of small intestine (A) and colon (B) were collected and Lgr5 GFP+ ISCs were detected by FACS R atios of Lgr5 GFP+ ISCs in total crypt cells were shown as scatter diagram. n =8 Lgr5 GFP mice for each panel. (C) 2 month old mice were treated with 5

HT inhibitor pCPA for 36 h and 72 h, and representative H& E images of small intestine (SI) and colon were shown in left panel. n 50 fields from five mice were observed and shown in right panel. (D) Lgr5 in situ hybridization w as performed in small intestine (SI) and colon tissues from pCPA treated mice. Typical i mage s were shown in left panel, and statistical result s of n 50 fields from five mice were in right panel. (E) pCPA treated m ice were treated with 10 Gy s radiation , and sacrifice d at indicated time points. Intestinal tissues were collected for H&E stainin g (upper panel). Numbers of intact crypts were shown in lower panel (means ±s.d). Five 2 month old mice were used and n =20 fields were taken for each group. F) Sert KO small intestine (SI) and colon crypts were collected for ISC detection by FACS. R atios o f Lgr5 GFP+ ISCs were shown. G) Lgr5 GFP CreERT2 Rosa26 lsl lacZ LR lacZ) mice were crossed with Sert mice, followed by administration of tamoxifen (TAM) for lineage tracing analysis through intestinal whole mount staining for β gal. n =7 mice were sacrifice d at indicated time points and typical jejunum sections on P65 (postnatal day 65) were shown. (H) LR lacZ Sert mice were used for lineage tracing analysis, and intestinal tissues were stained for lacZ observation. For C E , scale bars, 100 μm . P < 0.05, P < *** P < 0.001 by unpaired one tailed Student’s t test. At least three independent experiments were performed with similar results, and representative experiments were shown.

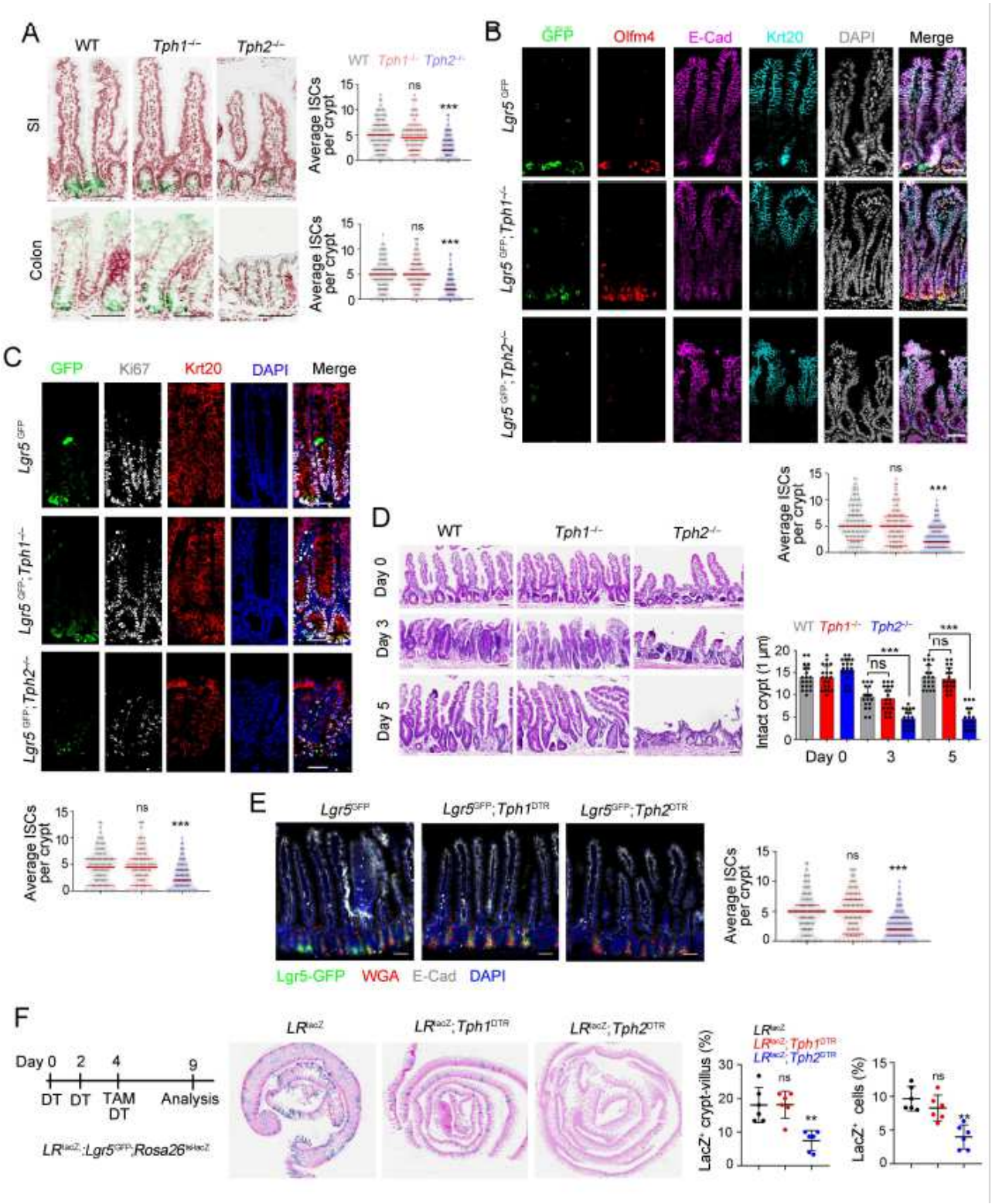

Figure 2

5 HT generated by enteric serotonergic neurons contributes to ISC self renewal. A) Lgr5 in situ hybridization w as performed in small intestine (SI) and colon tissues from Tph1 and Tph2 knockout mice . Typical image were shown in left panel, and n 50 fields from five mice were observed and shown in right panel. Scale bars, 100 μm . B , C) Lgr5 GFP Tph1 mice and Lgr5 GFP Tph2 mice were sacrifice d on P60 and intestine tissues were collected for immunofluorescence staining by indicated antibodies.

Typical 22 images of small intestine (B) and large intestine (C) are shown. Scale bar s , 50 μm . D) Tph1 and Tph2 knockout m ice were treated with 10 Gy s radiation , and sacrifice d at indicated time points. Intestinal tissues were collected for H&E staining (upper panel) and numbers of intact crypts were shown in lower panel (means ±s.d). n =20 fields from five mice were taken for each group. Scale bars, 100 μm (E) Fluorescence staining of intestinal tissue from 2 month old Lgr5 GFP , Lgr5 GFP Tph1 DTR and Lgr5 GFP Tph2 DTR mice 5 days after diphtheria toxin treatment . Scale bars, 5 0 μ m. (LR lacZ Tph1 DTR and LR lacZ Tph2 DTR mice were used for lineage tracing analysis, and intestinal tissues were stained for lacZ observation. * P < 0.05, P < *** P 0.001 by unpaired one tailed Student’s t test. At least three independent experiments were performed with similar results, and representative experiments were shown.

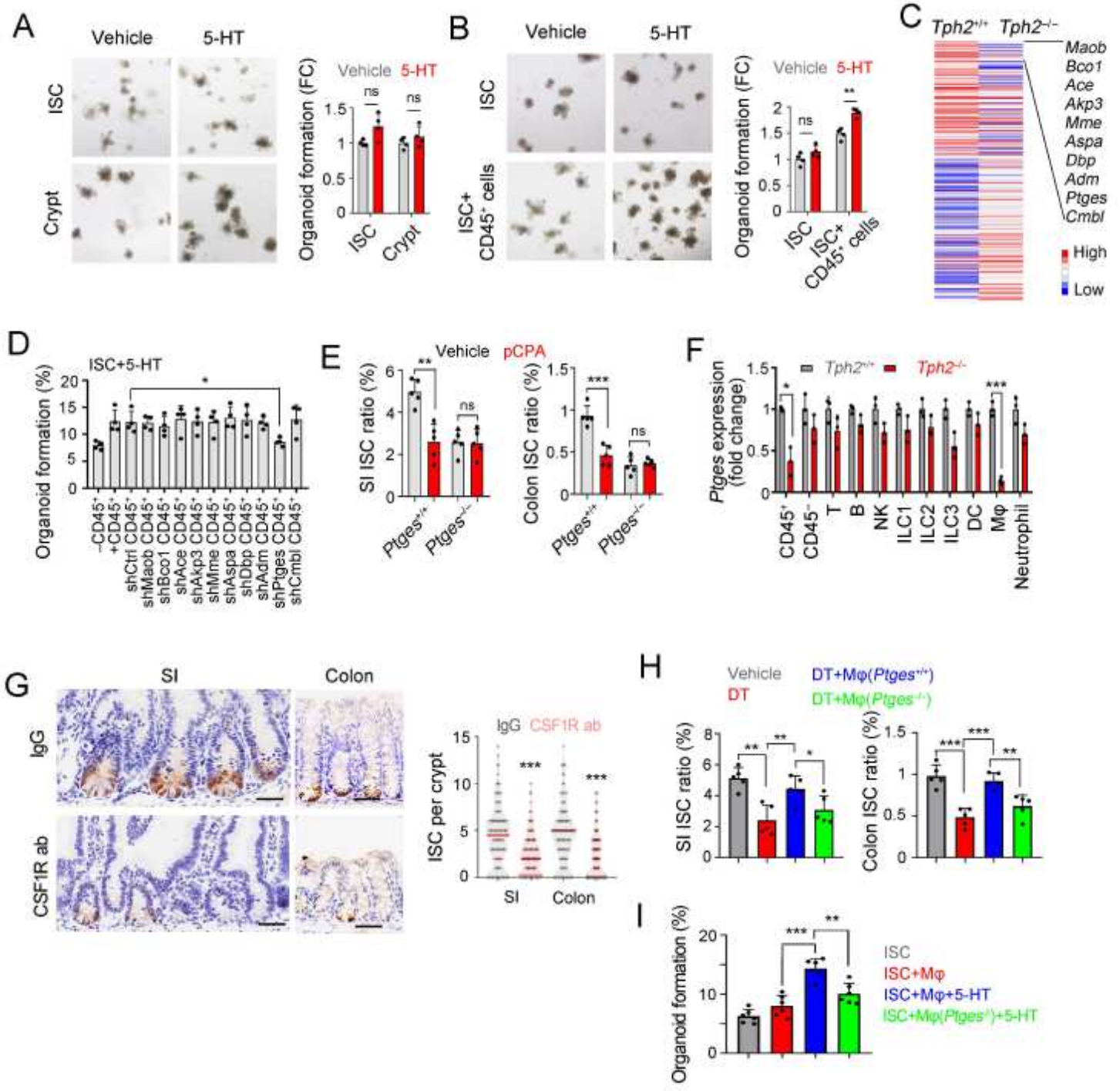

Figure 3

5 HT activates Ptges expression in macrophage s A , B) Organoid formation of ISC and crypt (A), or ISCs co cultured with CD45 cells (B) B). Organoid formation medium was supplemented with with o ut 5 HT. (C) Heat map of Tph2 knockout and control propria cells, with top10 lowly expressed genes in Tph2 knockout cells listed in right. Red , high expression; Blue, low expression. (D) Organoid formation ratios of ISCs co cultured with propria cells in which indicated genes were silenced individually. (E) ISC ratios of Ptges and Ptges mice, which were treated with pCPA 3 days before ISC detection. (F) Realtime PCR analysis for Ptges expression in indicated cells isolated from Tph2 and Tph2 mice. (G) Lgr5 in situ

hybridization in small intestine (SI) and colon tissues of macrophage depleted mice, which were treated with CSF1R ab (antibody) antibody). Scale bars, 50 μm H) FACS detection for ISC ratios in small intestine s (SI) and colon crypt s from indicated treated mice. (I) Organoid formation of ISCs, co cultured with WT or Ptges knockout macrophage s . Typical images were in left panel and organoid formation ratios in right panels. At least three independent experiments were performed with similar results, and representative experiments were shown.

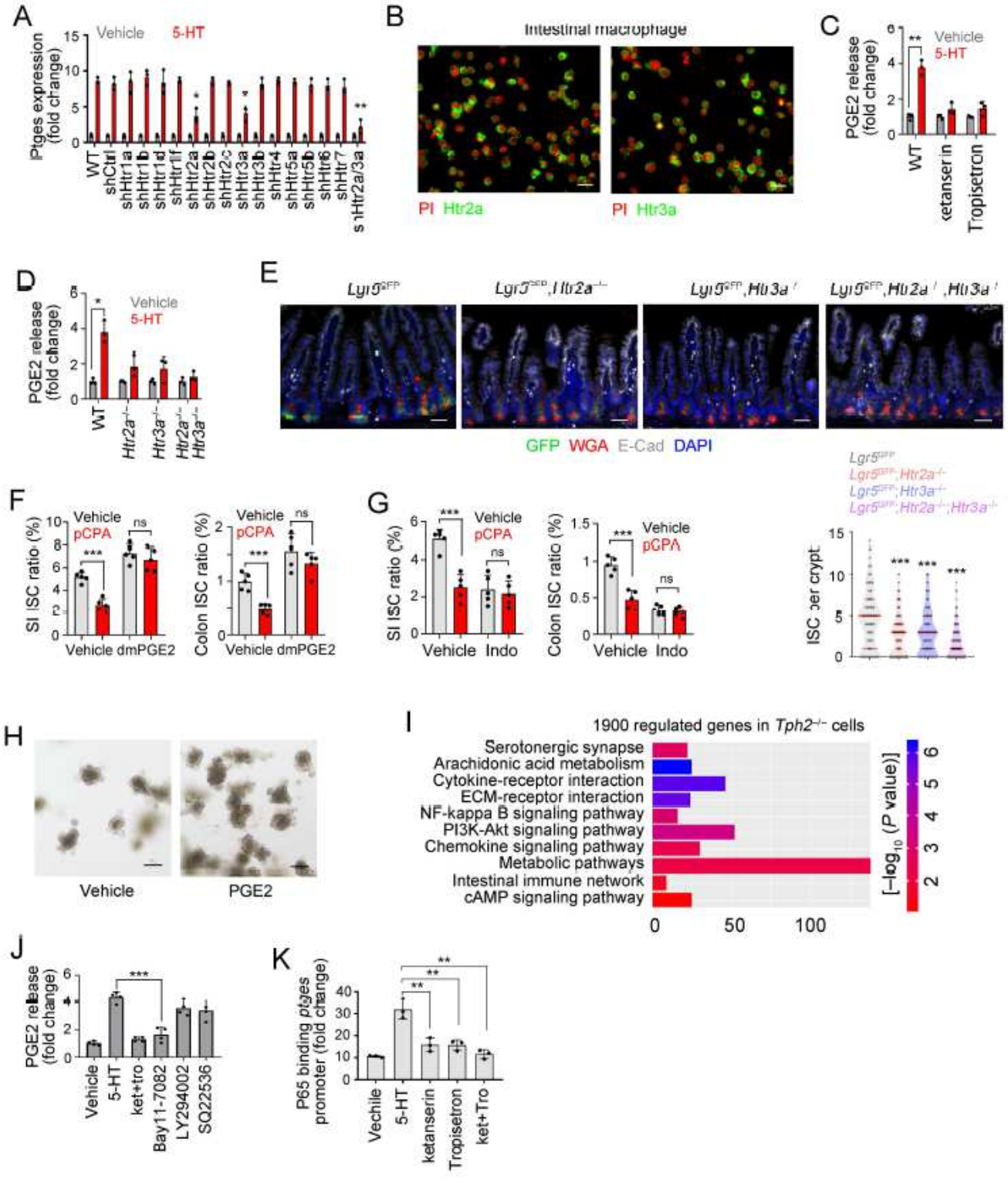

Figure 4

5 HT promotes PGE2 expression with engagement with its receptors Htr2a and Htr3a. (A) Realtime PCR for Ptges expression levels in 5 HT treated macrophages, in which the indicated 5 HT receptors were silenced individually. (High expression of Htr2a and Htr3a in intestinal macrophage cells , which were enriched via FACS. C) PGE2 production in macrophages treated with indicated inhibitors of 5 HT receptor. D) ELISA detection for PGE2 production in microphages, which were sorted from 5 HT treated Htr2a KO, Htr3a KO or D KO mice. All PGE2 levels were normalized to those of Vehicle treated mice. (Fluorescence staining of intestinal tissue from 2 month old Lgr5 GFP , Lgr5 GFP Ttr2a –//–, Lgr5 GFP Ttr3a and Lgr5 GFP Ttr2a Ttr3a mice. F , G) FACS detection for ISC ratios in small intestine (SI) or colon tissues from dmPGE2 treated (F) or indomethacin (Indo) treated (G) mice. H) Organoid formation of ISCs, supplemented with without PGE2. (I) Gene ontology analysis for pathway alterations in Tph2 and Tph2 cells. (J) ELISA detection for PGE2 production in indicated treated macrophage s . (K) Realtime PCR analysis to detect enrichment of Ptges promoter (3200~ 3000 fragment) in ChIP eluate, using P65 antibody and indicated treated macrophages. At least three independent experiments were performed with similar results, and representative experiments were shown.

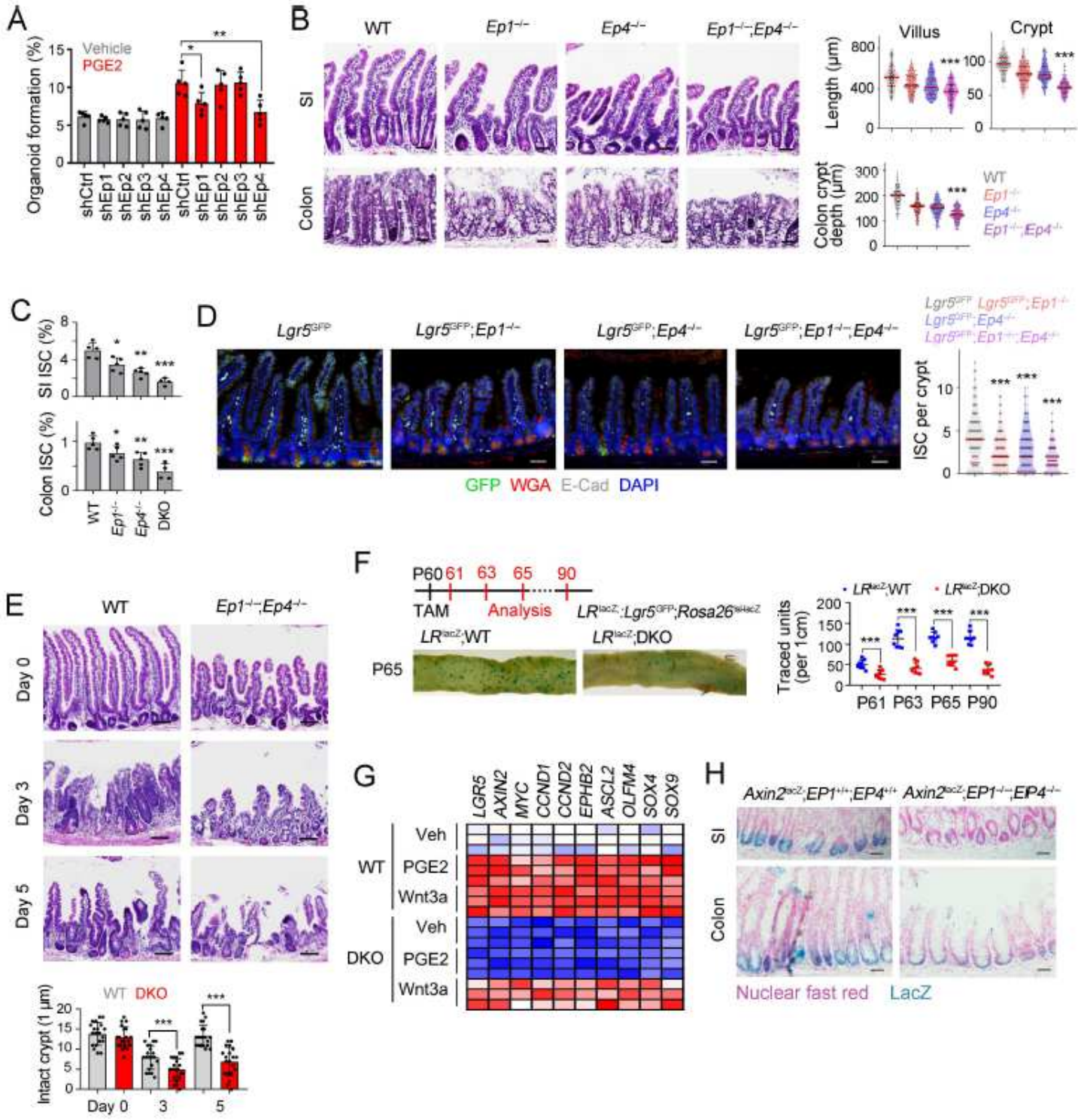

Figure 5

PGE2 drives Wnt signaling activation to maintain ISC stemness. (A) Orgnoid formation assay of indicated PGE2 receptor silenced ISCs, using PGE2 supplemented medium. B) H&E staining of small intestine (SI) and colon of WT, Ep1 –//–, Ep4 and D KO mice . Typical images were shown in left panel and n 50 fields were observed in right panel. Scale bars, 5 0 μm C) FACS detection for ISC ratios in small intestine (SI) and colon crypt, which were from WT, Ep1 –//–, Ep4 and D KO mice. D) Fluorescence staining of

intestinal tissue from 2 month old Lgr5 GFP , Lgr5 GFP Ep1 –//–, Lgr5 GFP Ep4 and Lgr5 GFP Ep1 Ep4 mice Scale bars, 5 0 μm E) WT and D KO mice were treated with 10 Gy's radiation, and sacrificed at indicated time points , and typical images were shown Scale bars, 100 μm . F) Lgr5 GFP CreERT2 Rosa26 lsl lacZ LR lacZ mice were crossed with D KO mice, and intestinal whole mount staining of β gal was performed for lineage tracing analysis. n 8 mice were observed for each group and typical jejunum sections were shown. G) Heatmap of indicated Wnt/β catenin target genes in WT and D KO ISCs. H WT and D KO mice were crossed with Axin2 lacZ mice. Small intestinal (SI) and colon tissues were stained for β gal expression. β gal staining indicates the activation of Wnt/ β catenin signaling. Scale bars, 50 μm . * P 0.05, P < *** P < 0.001 by unpaired one tailed Student's t test. At least three independent experiments were performed with similar results, and representative experiments were shown.

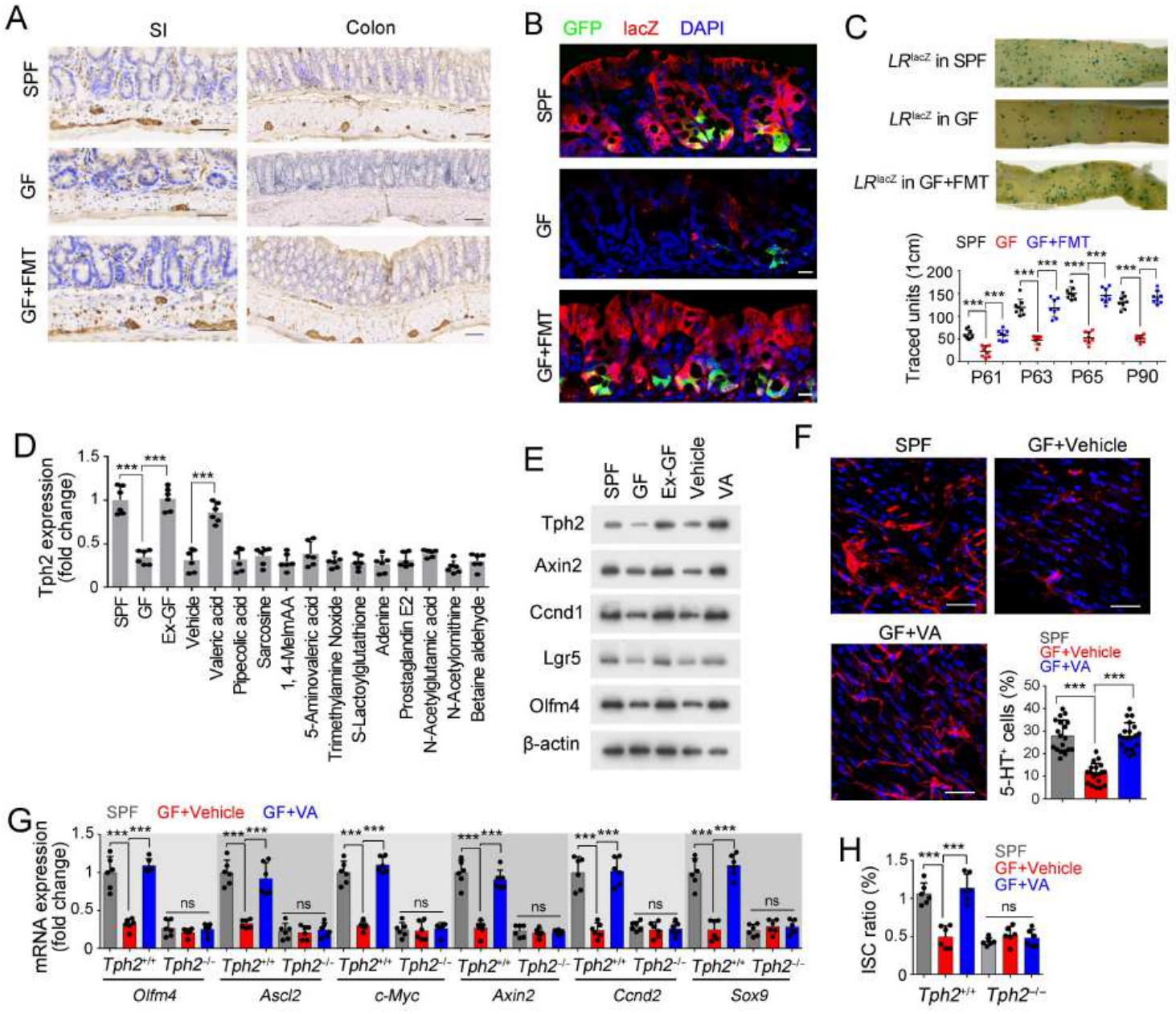

Figure 6

Microbiota promotes Tph2 expression to generate 5 HT. (SPF mice, GF mice and FMT into GF mice were used for Tph2 immunohistochemistry . Typical images of small intestine (SI) and colon tissues were shown. Scale bars, 100 μm . B) Lgr5 GFP CreERT2 Rosa26 lsl lacZ LR lacZ mice in SPF GF states and FMT into GF mice were treated with tamoxifen (TAM) for lineage tracing analysis. 5 days later, GFP and lacZ signals were detected by confocal microscopy. Scale bars, 20 μm . C) SPF, GF and FMT into GF LR lacZ mice were treated with TAM for lineage tracing analysis. n =8 mice were sacrifice d at indicated time points and typical jejunum sections on P65 were shown. Numbers of traced crypt villus units (blue plots) at indicated time points were shown in lower panel (means ±s.d). D) GF mice were treaded with indicated metabolite s, and Thp2 in intestine tissues was detected by realtime PCR. SPF and Ex GF mice were used for positive controls. (E) Total intestine tissues from treated mice were lyzed for Western blot. β actin was used as a loading control. (F) Myenteric plexus was isolated from treated mice, and 5 HT was detected by confocal microscopy. Typical images and 5 HT ratios were shown. Scale bars, 50 μm . G) Colon tissues from treated mice were used for realtime PCR analysis. ISC related genes (Olfm4, Ascl2) and β catenin target genes (c Myc, Axin2, Ccnd2, Sox9) were detected. H) Colon tissues were obtained from VA treated mice and ISCs were detected by FACS. Ratios of ISCs were shown.* P < 0.05, P < ***** P < 0.001 by unpaired one tailed Student’s t test. At least three independent experiments were performed with similar results, and representative experiments were shown.

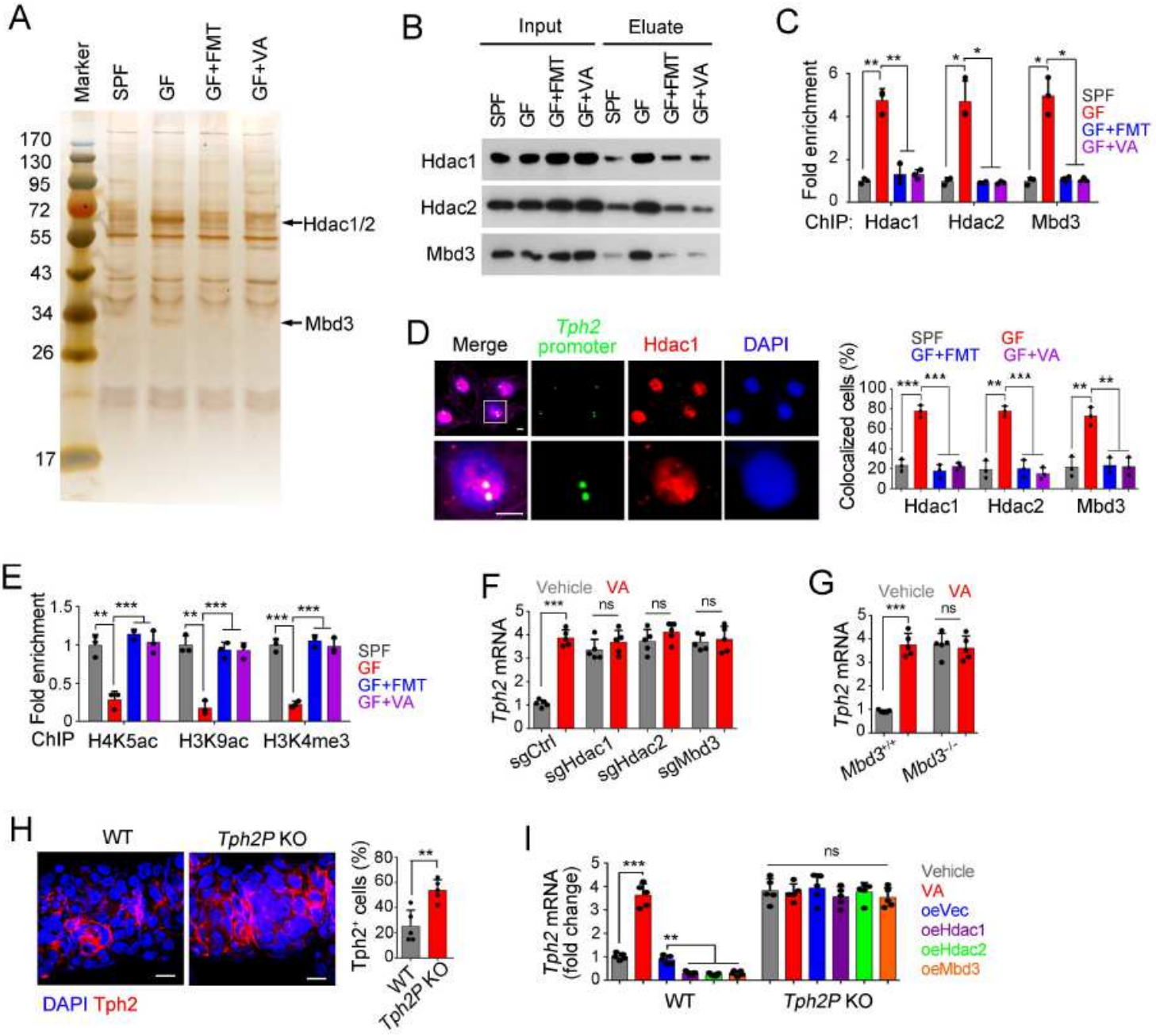

Figure 7

VA inhibits enrichment of the NuRD complex onto Thp2 promoter to initiate its expression . A) Silver staining of eluate from CAPTURE assay Capture of Chromatin Interactions by Biotinylated dCa s9) using SPF, GF and VA treated cells. Increased bands in GF cells were identified as Hdac1, Hdac2 and Mbd3. (B) The interaction of Tph2 promoter with Hdac1, Hdac2 and Mbd3 in indicated m yenteric plexus was detected by DNA pulldown and Western blot. (C) Indicated myenteric plexus cells were obtained for ChIP assay against Hdac1, Hdac2 and Mbd3. Enrichment of Thp2 promoter was examined by realtime PCR. (D) Enteric serotonergic neurons were sorted by Tph2, and confirmed by 5 HT staining, followed by FISH for Tph2 promoter detection and immunofluorescence staining for Hdac1 . Co localization of Tph2 promoter with Hdac 1 in enteric serotonergic neurons of GF mice was shown in left panel. Ratios of co

localized cells were shown in right panel. n =3 mice were used per panel, and 100 cells were observed per mouse. Scale bars, 4 μm E) H4K5ac, H3K9ac and H3K4me3 modification s of Thp2 promoter were detected by ChIP assay. 3600~ 3400 region of Thp2 promoter were detected by realtime PCR. (F, G) Hdac1 , Hdac2 and Mbd3 knockout cells were treated with VA, and Tph2 expression was detected by realtime PCR. (H) Rosa26 lsl Cas9 GFP mice were used for Tph2 promoter knockout (Tph2P KO), and then Tph2 expression was measured by confocal microscopy. Five Tph2P KO clones were established. Typical neurosphere images were shown in left panel and Tph2 cell ratios were shown in right panel. Scale bars, 10 μm I) Tph2 promoter (Tph2P) knockout cells were treated with VA or overexpressed the NuRD components, followed by Tph2 expression. * P < 0.05, P < *** P < 0.001 by unpaired one tailed Student's t test. At least three independent experiments were performed with similar results, and representative experiments were shown.

Supplementary Files

This is a list of supplementary files associated with this preprint. Click to download.

- 1SupplementaryFiguresXTablesFinal.pdf